Mon. Not. R. Astron. Soc. **000**, 000–000 (0000) Printed 18 April 2012 (MN LATEX style file v2.2)

Measuring mass-loss rates and constraining shock physics using X-ray line profiles of O stars from the *Chandra* archive

David H. Cohen,[1⋆] Emma E. Wollman,[1,2] Maurice A. Leutenegger,[3,4]
Jon O. Sundqvist,[5] Alex W. Fullerton,[6] Janos Zsargó[7] Stanley P. Owocki[5]
[1] *Swarthmore College, Department of Physics and Astronomy, Swarthmore, Pennsylvania 19081, USA*
[2] *Caltech, Department of Physics, 1200 East California Blvd., Pasadena, California 91125, USA*
[3] *NASA/Goddard Space Flight Center, Code 662, Greenbelt, Maryland 20771, USA*
[4] *CRESST and University of Maryland, Baltimore County, MD 21250, USA*
[5] *University of Delaware, Bartol Research Institute, Newark, Delaware 19716, USA*
[6] *Space Telescope Science Institute, 3700 San Martin Dr., Baltimore, Maryland 21218, USA*
[7] *Instituto Politécnico Nacional, Escuela Superior de Fisica y Matemáticas, C.P. 07738, Mexico, D.F., Mexico*

18 April 2012

ABSTRACT

We quantitatively investigate the extent of wind absorption signatures in the X-ray grating spectra of all non-magnetic, effectively single O stars in the *Chandra* archive via line-profile fitting. Under the usual assumption of a spherically symmetric wind with embedded shocks, we confirm previous claims that some objects show little or no wind absorption. However, other objects do show asymmetric and blue shifted line profiles, indicative of wind absorption. For these stars, we are able to derive wind mass-loss rates from the ensemble of line profiles, and find values modestly lower than theory predicts, and consistent with Hα if clumping factors of $f_{cl} \approx 20$ are assumed. The same profile fitting indicates an onset radius of X-rays typically at $r \approx 1.5\ R_*$, and terminal velocities for the X-ray emitting wind component that are consistent with that of the bulk wind. Both of these results are in agreement with the predictions of numerical simulations of embedded wind shocks due to the line-driving instability. We explore the likelihood that the stars in the sample that do not show significant wind absorption signatures in their line profiles have at least some X-ray emission that arises from colliding wind shocks with a close binary companion.

Key words: stars: early-type – stars: mass-loss – stars: winds, outflows – X-rays: stars

1 INTRODUCTION

By losing mass at a rate of $\dot{M} \sim 10^{-6}\ M_\odot\ yr^{-1}$ via its stellar wind, an O star can shed a significant portion of its mass over the course of its lifetime. Not only can this substantially reduce the mass of a core-collapse supernova progenitor, but the wind transfers a significant amount of mass, momentum, and energy to the surrounding interstellar medium. Thus, the wind mass-loss rate is an important parameter in the study of both stellar evolution and of the Galactic environment. In recent years there has been increased awareness of large systematic uncertainties in many mass-loss rate diagnostics, primarily due to wind clumping, rendering the actual mass-loss rates of O stars somewhat controversial (e.g. Hamann et al. (2008)).

⋆ E-mail: cohen@astro.swarthmore.edu

X-rays provide a potentially good clumping-insensitive mass-loss rate diagnostic via the effect of wind attenuation on X-ray emission line profile shapes. The characteristic line profile shape that provides the diagnostic power arises because red-shifted photons emitted from the rear hemisphere of the wind are subject to more attenuation than the blue-shifted photons originating in the front hemisphere (see figure 2 in Cohen et al. (2010a)). The degree of blue shift and asymmetry in these line profiles is then directly proportional to the wind column density and thus to the mass-loss rate. By fitting a simple quantitative model (Owocki & Cohen 2001) to each emission line in a star's spectrum and then analyzing the ensemble of line optical depths, we can determine the star's mass-loss rate (Cohen et al. 2010a, 2011).

Because this diagnostic scales with the column density rather than the square of the density, it avoids many of the problems presented by traditional mass-loss rate diagnos-

tics. In particular, density-squared diagnostics such as Hα and radio or IR free-free emission will overestimate the mass-loss rate if clumping is not accounted for. And even when clumping is accounted for, there is a degeneracy between the mass-loss rate and the clumping factor. UV absorption line diagnostics are problematic as well, due to their sensitivity to ionization corrections which are highly uncertain and which themselves also are subject to density-squared clumping effects. Recent, more sophisticated application of these diagnostics, assuming a radially dependent clumping factor, has led to a downward revision of the mass-loss rates of O stars (Bouret et al. 2005; Fullerton et al. 2006; Puls et al. 2006). These lowered mass-loss rates provide a natural explanation for the initially surprising discovery (Kahn et al. 2001; Cassinelli et al. 2001) that X-ray line profiles are not as symmetric as traditional mass-loss rate estimates had implied.

While small-scale, optically thin clumping reconciles the X-ray, UV, Hα, IR, and radio data for these stars, there is no direct evidence for large-scale, optically thick clumping, or porosity, in the X-ray data themselves (Cohen et al. 2008; Sundqvist et al. 2012; Leutenegger et al. 2012). Porosity results from optically thick clumps, which can "hide" opacity in their interiors, enhancing photon escape through the interclump channels. While porosity has been proposed as an explanation for the more-symmetric-than-expected observed X-ray line profiles (Oskinova et al. 2006), very large porosity lengths are required in order for porosity to have any effect on line profiles (Owocki & Cohen 2006), and levels of porosity consistent with measured line profiles produce only modest ($\sim$ 25 per cent) effects on derived mass-loss rates (Sundqvist et al. 2012; Leutenegger et al. 2012). In this paper, we derive mass-loss rates from the measured X-ray line profiles under the assumption that significant porosity is not present. *Co-authors: I'm not sure this paragraph belongs here in the intro. We could wait till the discussion to talk about porosity at all. What do you think?*

The initial application of the X-ray line profile based mass-loss rate diagnostic to the O supergiant ζ Pup gave a mass-loss rate of $\dot{M} = 3.5 \times 10^{-6}$ M$_\odot$ yr^{-1} (Cohen et al. 2010a). This represents a factor of three reduction over the unclumped Hα value (Repolust et al. 2004; Puls et al. 2006), and is consistent with the newer analysis of Hα, IR, and radio data which sets an upper limit of $\dot{M} < 4.2 \times 10^{-6}$ M$_\odot$ yr^{-1} when the effects of clumping are accounted for (Puls et al. 2006). A similar reduction is found for the very early O supergiant, HD 93129A, where the X-ray mass-loss rate of $\dot{M} = 6.8 \times 10^{-6}$ M$_\odot$ yr^{-1} is consistent with the observed Hα line if clumping is accounted for via $f_{cl} = 12$ (Cohen et al. 2011).

The goal of this paper is to extend the X-ray line-profile mass-loss rate analysis to all the non-magnetic, effectively single[1] O stars with grating spectra in the *Chandra* archive. It is already known that some, especially later-type, O stars show no obvious wind attenuation signatures (Miller et al. 2002; Skinner et al. 2008), and as one looks toward weaker winds in early B (V - III) stars, the X-ray lines are not as broad as the wind velocities would suggest they should be (Cohen et al. 2008). Therefore, we have excluded from our sample very late-O main sequence stars with relatively narrow lines, but we do include late-O giants and supergiants, even when the profiles appear unaffected by attenuation. In these cases we want to quantify the level of attenuation that may be hidden in the noise, placing upper limits on their mass-loss rates. Of course, it is possible that the model assumptions break down for some of the stars in the sample, not least of all if wind-wind interactions with a binary companion are responsible for some of the X-ray emission, in which case an intrinsically symmetric emission line profile may dilute whatever attenuation signal is present.

An additional goal of this paper is to constrain wind-shock models of X-ray production by extracting kinematic and spatial information about the shock-heated plasma from the line profiles. The profiles are Doppler broadened by the bulk motion of the hot plasma embedded in the highly supersonic wind. Our quantitative line-profile model allows us to derive an onset radius of hot plasma and also, for the highest signal-to-noise lines, the terminal velocity of the X-ray emitting plasma. We will use these quantities to test the predictions of numerical simulations of wind-shock X-ray production.

The paper is organized as follows: In the next section we describe the data and our sample of O stars taken from the *Chandra* archive. In §3 we describe our data analysis and modeling methodology including the line profile model, the line-profile fitting procedure, and the derivation of the mass-loss rate from an ensemble of line fits. In §4 we present our results, including mass-loss rate determinations for each star in our sample, and in §5 we conclude with a discussion of the implications of the line profile fitting results.

2 THE PROGRAM STARS

2.1 Observations

All observations reported on in this paper were made with *Chandra*'s High Energy Transmission Grating Spectrometer (HETGS) (Canizares et al. 2005). The HETGS has two grating arrays: the Medium and High Energy Gratings (MEG and HEG). The MEG has a resolution of 0.023 Å, while the HEG has a resolution of 0.012 Å, but lower sensitivity. We used the standard reduction procedure (CIAO 3.3 to 4.3) for most of the spectra, but for Cyg OB 8A, which is in a crowded field, care had to be taken to properly centroid the zeroth order spectrum of the target star, which necessitated the use of a customized reduction procedure within CIAO.

The observed spectra consist of a series of emission lines superimposed on a primarily bremsstrahlung continuum. The lines arise from high ionization states: most lines are from helium-like or hydrogen-like ions from abundant elements N through S, and the remainder come from iron L-shell transitions, primarily in Fe XVII, but also from higher stages, especially for stars with hotter plasma temperature distributions. *Chandra* is sensitive in the wavelength range from 1.2 to 31 Å (0.4 to 10 keV). However, the shortest-wavelength line we are able to analyze in our sample stars is the Si XIV line at 6.182 Å and the longest is the O VII line at 21.804 Å. The spectra vary in quality – from 1611 to 15514 total first-order MEG + HEG counts – and some suf-

[1] Effectively single in the sense that there is no obvious wind-wind interaction-related X-ray emission.

fer from significant interstellar attenuation at longer wavelengths. These two factors determine the number of lines we are able to fit in each star.

2.2 The sample

We selected every O and very early B star in the *Chandra* archive as of 2009 with a grating spectrum – see XATLAS (Westbrook et al. 2008) – that shows obviously wind-broadened emission lines, aside from ζ Pup and HD 93129A, which we have already analyzed (Cohen et al. 2010a, 2011). We eliminated from our sample those stars with known magnetic fields that are strong enough to provide significant wind confinement (this includes θ^1 Ori C and τ Sco) and we also excluded obvious binary colliding wind shock (CWS) X-ray sources, which are hard and variable (such as γ^2 Vel and η Car). Some objects remaining in the sample are possible CWS X-ray sources. They are included because their line profiles do not obviously appear to deviate from the expectations of the embedded wind shock (EWS) scenario, although we give special scrutiny to the fitting results for these stars in §5. We also exclude main sequence stars and giants with spectral type O9.5 and later, as these stars (including σ Ori A and β Cru) have X-ray lines too narrow to be understood in the context of standard embedded wind shocks. We ended up including one B star, the supergiant ϵ Ori (B0 Ia). The sample stars and their important parameters are listed in Table 1.

3 MODELING AND DATA ANALYSIS METHODOLOGY

3.1 X-ray emission line profile model

We use the model of X-ray emission and absorption introduced by Owocki & Cohen (2001). This model has the benefit of describing a general X-ray production scenario, making few assumptions about the details of the physical mechanism that leads to the production of shock-heated plasma in the wind. The model does assume that the cold, absorbing material in the wind and the hot, X-ray-emitting material both follow a β-velocity law of the form

$$v = v_\infty(1 - R_*/r)^\beta, \tag{1}$$

where v_∞, the terminal velocity of the wind, usually has a value between 1500 and 3500 km s^{-1}. The β parameter, derived from Hα and UV lines, typically has a value close to unity. The model also assumes that the filling factor of X-ray emitting plasma is zero below some onset radius, R_o, and is constant above R_o. Our implementation of the X-ray line profile model[2] optionally includes the effects of porosity (Oskinova et al. 2006; Owocki & Cohen 2006) and of resonance scattering (Leutenegger et al. 2007) on the individual line profile shapes. We explore both effects for a subset of stars in our sample.

[2] The XSPEC custom model, *windprofile*, is publicly available at heasarc.gsfc.nasa.gov/docs/xanadu/xspec/models/windprof.html.

The adjustable free parameters of the profile model are generally just the normalization, the parameter that describes the onset radius of X-ray production, R_o, and a fiducial optical depth parameter, τ_*, which we describe below. For a few high signal-to-noise lines, we allow v_∞, the wind terminal velocity, to be a free parameter of the fit as well. Otherwise, we fix this parameter at the value listed for the star in Table 1. The parameter R_o controls the widths of the line via the assumed wind kinematics represented by eqn. 1. Small values of R_o correspond to more X-ray production close to the star where the wind has a small Doppler shift, while large values of R_o indicate that most of the X-rays come from high Doppler shift regions in the outer wind. Hydrodynamic models show shocks developing about half a stellar radius above the surface of the star – albeit with some variation based on treatments of the line force parameters and of the lower boundary conditions in numerical simulations (Feldmeier et al. 1997; Runacres & Owocki 2002) – so we should expect R_o to be roughly 1.5 R_*.

The optical depth of the wind affects the blue shift and asymmetry of the line profile. The optical depth at a given location in the wind, and thus at a given wavelength, is proportional to the constant τ_*, given by

$$\tau_* = \frac{\kappa \dot{\mathrm{M}}}{4\pi R_* v_\infty}. \tag{2}$$

This constant appears in the exact expression for the optical depth at any arbitrary point in the wind,

$$\tau(p,z) = \int_z^\infty \kappa\rho(r')\mathrm{d}z' = \tau_* \int_z^\infty \frac{R_*\mathrm{d}z'}{r'^2(1 - R_*/r')^\beta}, \tag{3}$$

where p, z are the usual cylindrical coordinates: the impact parameter, p, is the projected distance from the z-axis centered on the star and pointing toward the observer, and $r \equiv \sqrt{p^2 + z^2}$.The second equality arises from substituting the β-velocity law into the general equation for the optical depth and employing the mass continuity equation. The value of τ_* controls the degree of asymmetry and blue shift of each line profile. The profile is calculated from

$$L_\lambda \propto \int_{R_o}^\infty \eta e^{-\tau}\mathrm{d}V, \tag{4}$$

where η is the X-ray emissivity, τ is calculated using eqn. 3, and the volume integral is performed over the entire wind above $r = R_o$. In addition to scaling with the mass-loss rate, τ_* is proportional to κ, the atomic opacity, and is thus dependent on wavelength. Note that the atomic opacity is effectively constant across a given line profile but it varies from line to line. We discuss the wind opacity further in §3.3.

3.2 Fitting procedure

All model fitting was done in XSPEC (v12.3 to 12.6). We fit the positive and negative first order spectra simultaneously, but not coadded. Coadded spectra are shown in the figures for display purposes, however. When there were a significant number of counts in the HEG measurements of a given line, we included those data in the simultaneous fit. In most cases there were negligible counts in the HEG data and we fit only the MEG data. Because Poisson noise dominates these low-count *Chandra* data, we could not use χ^2 as the fit statistic, and instead used the C statistic (Cash 1979). As with χ^2,

Table 1. Properties of Program Stars

Star	Spectral Type	$T_{\rm eff}$ (kK)	R ($R_\odot$)	log g (cm s^{-2})	v_∞ (km s^{-1})	MEG counts	HEG counts	exposure time (ksec)
HD 93250	O3.5 V	46.0	15.9	3.95	3250	6169	2663	193.7
9 Sgr	O4 V	42.9	12.4	3.92	3100	4530	1365	145.8
HD 150136	O5 III	40.3	15.1	3.69	3400	8581	2889	90.3
Cyg OB2 8A	O5.5 I	38.2	27.0	3.56	2650	6575	1892	65.1
HD 206267	O6.5 V					1516	419	73.5
15 Mon	O7 V	37.5	9.9	3.84	2150	1621	393	99.8
ξ Per	O7.5 III	35.0	14.0	3.50	2450	5603	1544	158.8
τ CMa	O9 II	31.6	17.6	3.41	2200	1300	311	87.1
ι Ori	O9 III	31.4	17.9	3.50	2350	4836	1028	49.9
ζ Oph	O9 V	32.0	8.9	3.65	1550	5911	1630	83.8
δ Ori	O9.5 II	30.6	17.7	3.38	2100	6144	1071	49.1
ζ Ori	O9.7 Ib	30.5	22.1	3.19	1850	11018	2496	73.4
ϵ Ori	B0 Ia	27.5	32.4	3.13	1600	6813	1474	91.7

Co-authors: We need stellar parameters for HD 206267, and I still need to put in the sources for all of these parameters (Emma had them in her draft, there are a couple that need to be corrected, but I've just left them all out here to save time; I'll compile them during the next editing iteration).

a lower C value indicates a better fit, given the same number of degrees of freedom. We assessed goodness-of-fit via Monte Carlo simulations of the distribution of the C statistic for each line fit. For placing confidence limits on model parameters, ΔC is equivalent to $\Delta\chi^2$ with a ΔC value of 1 corresponding to a 68 per cent confidence bound in one dimension (Press et al. 2007). We establish confidence bounds on the model parameters of interest one at a time, allowing other parameters to vary while establishing these bounds. There is generally a mild anti-correlation between $R_{\rm o}$ and τ_*, so we also examined the joint constraints on two parameters, adjusting the corresponding value of ΔC accordingly. Joint confidence limits are shown in Fig. 1, along with the best-fit models, for the Fe XVII line at 15.014 Å for several stars with varying degrees of wind signature strength.

To account for the weak continuum under each emission line, we first fit a region around the line with a continuum model having a constant flux per unit wavelength. This continuum model was added to the line-profile model when fitting the line itself. The fitting was generally then done with three free parameters: τ_*, $R_{\rm o}$, and a normalization factor. We fixed β at 1, and v_∞ at the value given in Table 1. A discussion of the effects of changing β and v_∞ as well as sensitivity to continuum placement, treatment of blends, and other aspects of our analysis can be found in Cohen et al. (2010a). One additional effect we account for is the radial velocity of each star. This effect was only significant for ξ Per, which has $v_r = 57$ km s^{-1} (Hoogerwerf et al. 2001).

The hydrogen-like Lyα lines in the spectra consist of two blended lines with wavelength separations that are much smaller than the resolution of the *Chandra* gratings. We fit these lines with a single model centered at the emissivity-weighted average of the two wavelengths. In some cases, the lines we wish to analyze are blended. If the blending is too severe to be modeled, as it is for the O VIII Lyβ line at 16.006 Å, we excluded the line from our analysis entirely. If the blended portion of the line could be omitted from the fit range without producing unconstrained[3] results, we simply fit the model over a restricted wavelength range. The Ne X Lyα line at 12.134 Å, for example, produces well-constrained results, even when its red wing is omitted due to blending with longer-wavelength iron lines. If lines from the same ion are blended, such as the Fe XVII lines at 16.780, 17.051, and 17.096 Å, we fit three models to the data simultaneously, constraining the τ_* and $R_{\rm o}$ values to be the same for all the lines in the blended feature. In the case of the aforementioned iron complex, we also constrained the ratio of the normalizations of the two lines at 17.096 and 17.051 Å, which share a common lower level, to the theoretically predicted value of 0.9 (Mauche et al. 2001) because the blending is too severe to be constrained empirically.

The helium-like complexes are among the strongest lines in many of the sample stars' spectra, but they are generally heavily blended. The forbidden-to-intercombination line intensity ratios are a function of the local mean intensity of the UV radiation at the location of the X-ray emitting plasma (Leutenegger et al. 2006). And so the spatial (and thus velocity) distribution of the shock-heated plasma affects both the line intensity ratios and the line profile shapes. We model these effects in tandem and fit all three line profiles, including the relative line intensities, simultaneously, as described in Leutenegger et al. (2006). In order to do this, we use UV fluxes taken from TLUSTY (Lanz & Hubeny 2003) model atmospheres appropriate for each star's effective temperature and log g values, as listed in Table 1. This procedure generates a single τ_* value and a single $R_{\rm o}$ value for the entire complex, and where $R_{\rm o}$ affects both the line shapes and the f/i ratios. We generally had to exclude the results for Ne IX due to blending with numerous irons lines.

[3] Unconstrained in the sense that the ΔC criterion does not rule out significant portions of model parameter space.

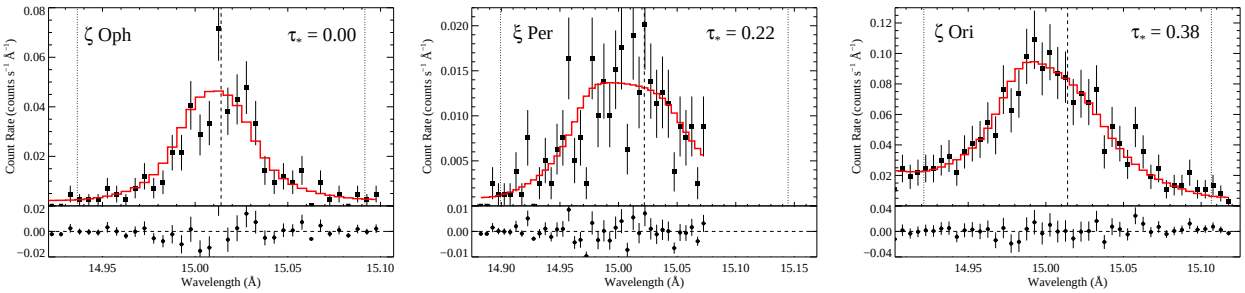

Figure 1. The Fe XVII line at 15.014 Å with best-fit model for three of the sample stars (ζ Oph, $\tau_* = 0.00^{+.01}_{-.00}$ (left), ξ Per, $\tau_* = 0.22^{+.14}_{-.12}$ (middle), and ζ Ori, $\tau_* = 0.38^{+.13}_{-.11}$ (right)) showing various degrees of asymmetry. The vertical dashed lines on the profile plots represent the laboratory line rest wavelength and the wavelengths corresponding to the terminal velocity of the wind. Note that the x-axis in each figure encompasses the same *velocity* range, but different wavelength ranges, due to the different terminal velocities of the three stars' winds. The emission line in ζ Oph is therefore even narrower, in an absolute sense, than it appears here. *Co-authors: I'm working on the contour plots showing the 2-D confidence regions in τ_*-R_o parameter space.*

3.3 Analyzing the ensemble of line fits from each star

To extract the mass-loss rate from a single derived τ_* parameter value, a model of the opacity of the cold, unshocked component of the wind is needed. Then, along with values for the wind terminal velocity and stellar radius, eqn. 2 can be used to derive a mass-loss rate for a given line. To derive a single mass-loss rate from an ensemble of emission lines, each with their own τ_* value, as we do here, the wavelength dependence of the τ_* values is assumed to follow the wavelength dependence of the atomic opacity, and eqn. 2 is solved for the best $\tau_*(\lambda)$, with $\dot{M}$ as the only free parameter. Although this correlation between $\tau_*(\lambda)$ and $\kappa(\lambda)$ was not noted in the initial analyses of *Chandra* grating spectra, it has recently been shown for the high signal-to-noise spectrum of ζ Pup that if all lines in the spectrum are considered – but blends that cannot be modeled are excluded – and a realistic model of the wavelength-dependent wind opacity is used, then the wavelength trend in the ensemble of τ_* values is consistent with the atomic opacity (Cohen et al. 2010a). For other stars, the wavelength trend of τ_* expected from $\kappa(\lambda)$ may not be evident, but may still be consistent with it, as has been shown, recently, for HD 93129A (Cohen et al. 2011).

The opacity of the bulk, unshocked wind is due to bound-free absorption (inner shell photoionization), and the contributions from N, O, and Fe are dominant, with important contributions from Ne and Mg at wavelengths below about 12 Å. The wind opacity is affected by the elemental abundances – both the overall metallicity and also the relative contributions of specific elements, most notably N and O, which are altered by CNO processing – and, to a lesser extent, by the ionization distribution in the wind.

In general, there do not exist precise abundance determinations for most of the stars in our sample, which are of course difficult to carry out and prone to systematic errors. The expectation is that these massive stars have metallicities close to solar, and that some, but not all, have enhanced nitrogen and depleted carbon and oxygen. Thus, we have calculated two generic wind opacity models: one using solar (Asplund et al. 2009) abundances and one that uses overall solar metallicity but has N at three times solar, O at 0.5 solar, and C at 0.25 solar. Note that the sum of the absolute C, N, and O abundances are, in this case, solar, even though the individual elemental abundances are not. We refer to these as the "solar" and "CNO processed" wind opacity models. Both assume an ionization balance based on O star models in (MacFarlane et al. 1994), but the opacity is largely insensitive to reasonable changes in the ionization distribution. *Co-authors/Janos: maybe we can elaborate on this. Perhaps by calculating or estimating the ionization balance of O, N, Ne, and Fe for some stars with large $T_{\rm eff}$ differences and making at least one more wind opacity model, with different ionization balance(s).* We show these two opacity models in Fig. 2. Note that from 5 to 20 Å, the two models are nearly identical. At 20 Å, however, the oxygen K-shell edge is stronger in the solar model than in the CNO-processed model. The only line that we are able to model longward of the oxygen edge is the O VII line complex near 21.7 Å. This complex is not very strong in any of our sources, but with higher signal-to-noise data, it could be possible to use it to differentiate between the two opacity models, and even measure the nitrogen abundance in the wind. Because of the similarity of the two opacity models, we use only the solar model in this paper. And we note that future determinations of the metallicity of any of the program stars can be accommodated by simply scaling the derived mass-loss-rate up or down by the reciprocal of the metallicity.

4 RESULTS

For each star in our sample, the simple line-profile model provides good fits to most of the emission lines and line complexes from which we are able to derive values for τ_* and R_o, using the formalism described in the previous section. In itself, this does not confirm the EWS scenario of X-ray production for each of the sample stars, as profile models with $\tau_* \approx 0$, at the spectral resolution of the *Chandra* gratings, are indistinguishable from a Gaussian, with the profile width controlled by the R_o parameter rather than the Gaussian σ. Rather, reasonable values of τ_* and R_o, and consistency between the τ_* values and the wavelength dependence of the atomic opacity of the wind are the minimum requirements to conclude that the EWS mechanism is operating in a given star and to interpret the ensemble τ_* values in the context of a mass-loss rate measurement.

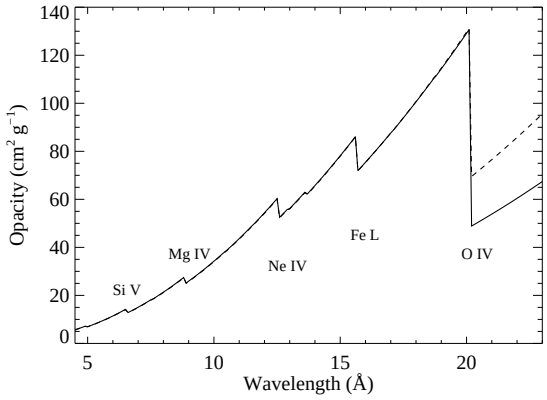

Figure 2. We present two different models for the wavelength-dependent opacity of the bulk wind, with the same simplified ionization balance assumed in each case, but altered C, N, and O abundances for the model shown as a dashed line. Prominent ionization edges are labeled.

There are three stars in the sample for which the data quality are not good enough to draw any meaningful conclusions: HD 206267, 15 Mon, and τ CMa. These are the three data sets with fewer than 2500 total MEG + HEG counts, and for none of these stars are there more than three emission lines for which profile fits with even marginal constraints can be made (and for none of the stars is there more than one weak line that is not potentially subject to resonance scattering and the associated ambiguity of model interpretation). We will not discuss these stars further in this paper. A fourth star, HD 93250, has only three usable lines, although it has a significantly larger number of counts in its spectra than the three stars we are excluding. *Co-authors: I have to take another look at the He-like complexes, which we don't have results for, for some reason.* The small number of strong lines, despite the higher signal-to-noise spectra, can be understood in the context of the high plasma temperature and correspondingly strong bremsstrahlung continuum and weak lines in the HD 93250 spectra. As we discuss in the next section, this is a strong indication that the X-ray spectrum of HD 93250 is dominated by hard X-ray emission from colliding wind shocks in the context of the binary wind-wind interaction mechanism.

We summarize the fitted τ_* and R_o values, and their uncertainties, in Figs. 3 and 4, respectively, and in Table 2. In these two figures, each point represents the fit to a single line or blended line complex. In Fig. 3 we also show the expected run of τ_* vs. λ given the theoretical mass-loss rates (Vink et al. 2000) listed in Table 2, as well as those we derive from fitting the mass-loss rates to the τ_* values. We show all ten sample stars, even though, as we will discuss in the next section, we discount the interpretation of these results in terms of a wind mass-loss rate for some of the stars. All ten of the mass-loss rate fits are formally good, with ξ Per showing the most scatter and largest reduced χ^2, but not large enough for the fit to be formally rejected.

Among the complications of the line-profile fitting is the effect of resonance scattering in optically thick X-ray lines. Leutenegger et al. (2007) showed that this effect is significant for oxygen and nitrogen lines in the *XMM-Newton* spectrum of ζ Pup. And those authors presented a ranking of the Sobolev optical depths expected for many strong lines in the *Chandra* bandpass. In our sample stars, the lines most likely to be affected by resonance scattering are Fe XVII at 15.014 Å, O VIII Lyα at 18.969 Å, and the resonance line at 21.602 Å in the O XVII He$_\alpha$ complex. For the spectrum of ϵ Ori, where resonance scattering seems to be important (see §5.1.10), we refit several of the lines, including these three, allowing the Sobolev optical depth to be a free parameter and the velocity law β of the hot plasma to be either $\beta_{Sob} = 0$ or 1 (Leutenegger et al. 2007) . Unfortunately, with those additional free parameters of the model, the values of the parameters we are interested in – τ_* and R_o – were nearly unconstrained. To account for the possible effects of resonance scattering, then, we eliminated the effected lines from the mass-loss rate determination (and from Figs. 3 and 4). These include all three lines mentioned above for ϵ Ori and also the O VIII Lyα line and the O VII He$_\alpha$ resonance line for ζ Ori. Note that in both cases, we were able to include the O VII intercombination line at 21.804 Å, which is not optically thick to resonance scattering, while excluding the nearby resonance line[4]. Excluding these lines from the mass-loss rate fits for these two stars led to higher mass-loss rates of a factor of 3 for ϵ Ori and 50 percent for ζ Ori. For no other star did accounting for resonance scattering make a significant difference for the mass-loss rate determination.

Co-authors: I will fit a few of the strongest lines with a model that includes anisotropic porosity and, likely, show that it can be ruled out as an important effect. I think that this subject warrants a paragraph or two. What do you think?

There are a small number of lines for which the fits are only of marginal quality or which provide suspect results. These include the Si XIII complex in ζ Ori, for which the fit is not formally good, the line shapes look unusually peaked, and the formal upper limit on τ_* is remarkably small. Other suspect fits include a few of the Ne IX complexes, which are probably affected by blending with numerous iron lines. For δ Ori, there is some indication that the lines are mildly red-shifted (rather than showing the expected net blue shift due to wind absorption). This is likely due to binary orbital motion of the primary. The results we show in Figs. 3 and 4 include a redshift (the magnitude of which was allowed to be a free parameter) in the two longest-wavelength lines for this star. We discuss this result for δ Ori, and the interpretation of the results for each individual star, in the following section.

We fit an average R_o value for each star based on the ensemble of line-fit results, and we show that average, and its 68 per cent confidence limits, in Fig. 4. For many of the stars, a single value provides a good fit, but for HD 150136, ι Ori, δ Ori, ζ Ori, and ϵ Ori the fits are marginal (rejected at $\approx$ 95 per cent confidence). For these latter two stars, at least, there is a modest correlation between R_o and wavelength. Finally, for a few lines in some of the sample stars' spectra, we treat the wind terminal velocity, v_∞, as a free parameter (as described in §3.2). These results are shown in Fig. 4 and

[4] Note that the resonance lines are more symmetric and have lower best-fit τ_* values than do the intercombination lines, which is consistent with the effect of resonance scattering being significant.

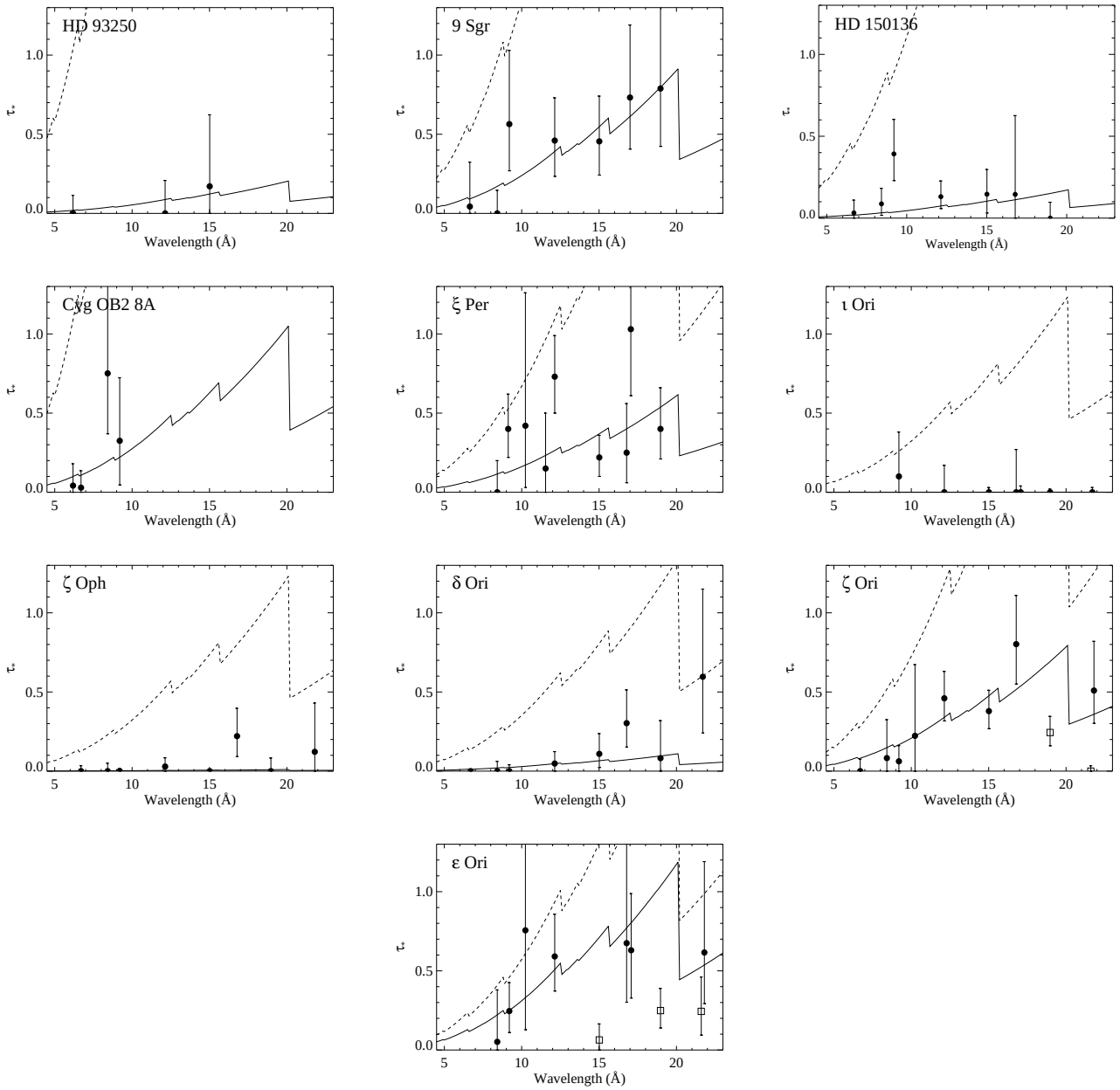

Figure 3. The fitted τ_* values (points), along with the 68 per cent confidence limits (error bars). The mass-loss rates derived from these values are shown graphically as the solid line, while the dashed line in each panel represents the τ_* trend expected from the theoretical mass-loss rates listed in Table 2. For ζ Ori and ϵ Ori we show the two and three points, respectively, omitted from the mass-loss rate fits because of resonance scattering (open squares). Note that in both stars, the He-like resonance line (at 21.602 Å) has a smaller τ_* value than the intercombination line (at 21.804 Å), which is indicative of resonance scattering being important.

listed in Table 3. For all four stars, we fit a single v_∞ value to the ensemble of line results, and in each case the fit is formally good.

5 DISCUSSION AND CONCLUSIONS

While the empirical line profile model provides good fits to nearly all the lines in all the sample stars, one of the primary results of this study is the overall weakness – or even absence – of wind absorption signatures in the *Chandra* grating spectra of O stars. This has been noted before by various authors examining individual objects, generally via fitting Gaussian profile models (e.g. Miller et al. (2002)), but here we have systematically quantified this result using a more physically meaningful line-profile model. There are three classes of explanations for the weak wind-absorption signatures we measure: (1) the line profile model is missing some crucial physics; (2) processes other than embedded wind shocks are contributing to the X-ray line emission and thereby diluting the characteristic shifted and skewed pro-

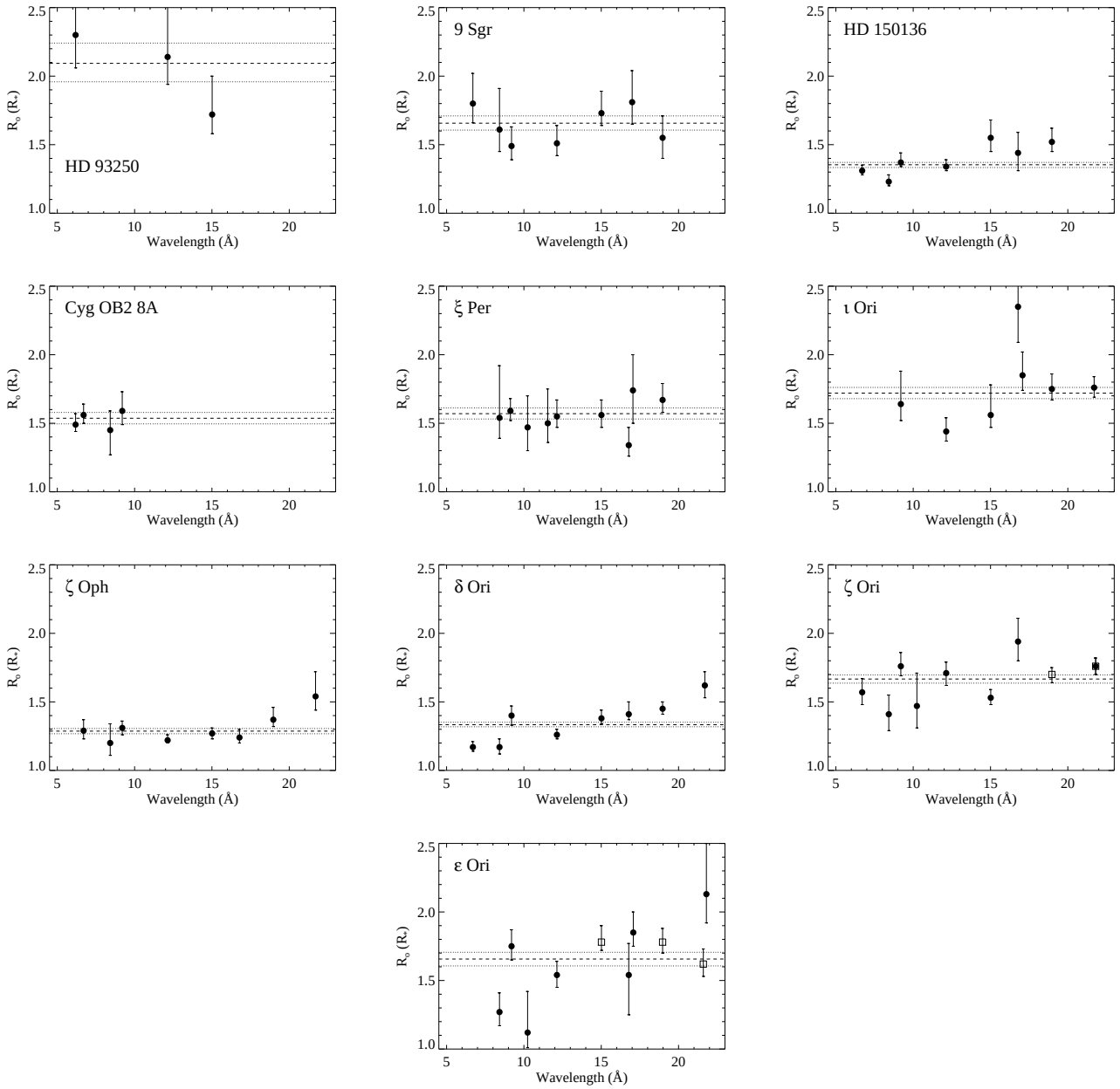

Figure 4. The fitted R_o values for each line in each sample star (filled circles), along with the 68 per cent confidence limits (error bars). The best-fit global R_o value for each star is indicated in each panel by the dashed line, while the dotted lines indicate the extent of the 68 per cent confidence limits. The excluded lines for ζ Ori and ϵ Ori are shown as open squares.

files that are the signature of wind absorption; and (3) the actual mass-loss rates of these stars are lower than expected.

Examining the trends in τ_* and R_o shown in Figs. 3 and 4, we can identify several stars with extremely low wind optical depths and/or shock onset radii that deviate significantly from the expectations of the embedded wind shock scenario. These include HD 93250, HD 150136, ι Ori, ζ Oph, and δ Ori. As we show below, it is likely that nearly all of these stars, and also Cyg OB2 8A, have a significant contribution from colliding wind shocks in their observed X-ray line profiles. The other stars in the sample: 9 Sgr, ξ Per, ζ Ori, and ϵ Ori have line profiles that are consistent with the expectations of the embedded wind shock scenario, with $R_o \approx 1.5\ R_*$ and τ_* values that, while low, are well within an order of magnitude of the expected values and are consistent with the expected wavelength trend of the atomic opacity of their winds.

The mass-loss rates we derive for these four stars from their ensembles of τ_* values are listed in Tab. 2 and are generally a factor of a few lower than the theoretical values computed by Vink et al. (2000). We summarize the X-ray-derived mass-loss rates for all the stars in the sample (even those for which the derived values cannot be trusted) in Fig. 6, and compare these mass-loss rates to the theoretical values. We also include ζ Pup and HD 93129A in this figure, as the X-ray line profiles of those two O supergiants were

Table 2. X-ray Derived Results for Each Star

Star	Spectral Type	$\dot{M}_{\rm theory}$ ($M_\odot$ yr^{-1})	$\dot{M}$ ($M_\odot$ yr^{-1})	χ^2	N_{lines}	$R_{\rm o}$ (R_*)	χ^2	primarily EWS?
HD 93250	O3.5 V	6.0×10^{-6}	$1.2^{+1.5}_{-1.2} \times 10^{-7}$	0.3	3	$2.09^{+.15}_{-.13}$	2.6	no
9 Sgr	O4 V	2.1×10^{-6}	$3.7^{+1.0}_{-0.9} \times 10^{-7}$	3.3	7	$1.66^{+.05}_{-.05}$	5.8	yes
HD 150136	O5 III	2.3×10^{-6}	$9.4^{+4.0}_{-4.1} \times 10^{-8}$	8.8	7	$1.35^{+.02}_{-.02}$	17.6	no
Cyg OB2 8A	O5.5 I	8.7×10^{-6}	$8.0^{+5.1}_{-5.1} \times 10^{-7}$	3.0	4	$1.54^{+.04}_{-.04}$	1.2	no
ξ Per	O7.5 III	9.3×10^{-7}	$2.2^{+0.6}_{-0.5} \times 10^{-7}$	11.0	9	$1.57^{+.05}_{-.04}$	5.3	yes
ι Ori	O9 III	5.5×10^{-7}	$3.2^{+84.}_{-3.2} \times 10^{-10}$	1.0	7	$1.72^{+.04}_{-.04}$	16.2	no
ζ Oph	O9 V	1.8×10^{-7}	$1.5^{+2.8}_{-1.5} \times 10^{-9}$	4.7	8	$1.29^{+.02}_{-.02}$	13.4	maybe
δ Ori	O9.5 II	5.3×10^{-7}	$4.3^{+2.6}_{-2.2} \times 10^{-8}$	6.3	8	$1.33^{+.02}_{-.01}$	52	no
ζ Ori	O9.7 Ib	1.2×10^{-6}	$3.4^{+0.6}_{-0.6} \times 10^{-7}$	5.5	8	$1.67^{+.03}_{-.03}$	18.4	yes
ϵ Ori	B0 Ia	1.2×10^{-6}	$6.5^{+1.1}_{-1.5} \times 10^{-7}$	1.2	7	$1.66^{+.05}_{-.05}$	22.1	yes

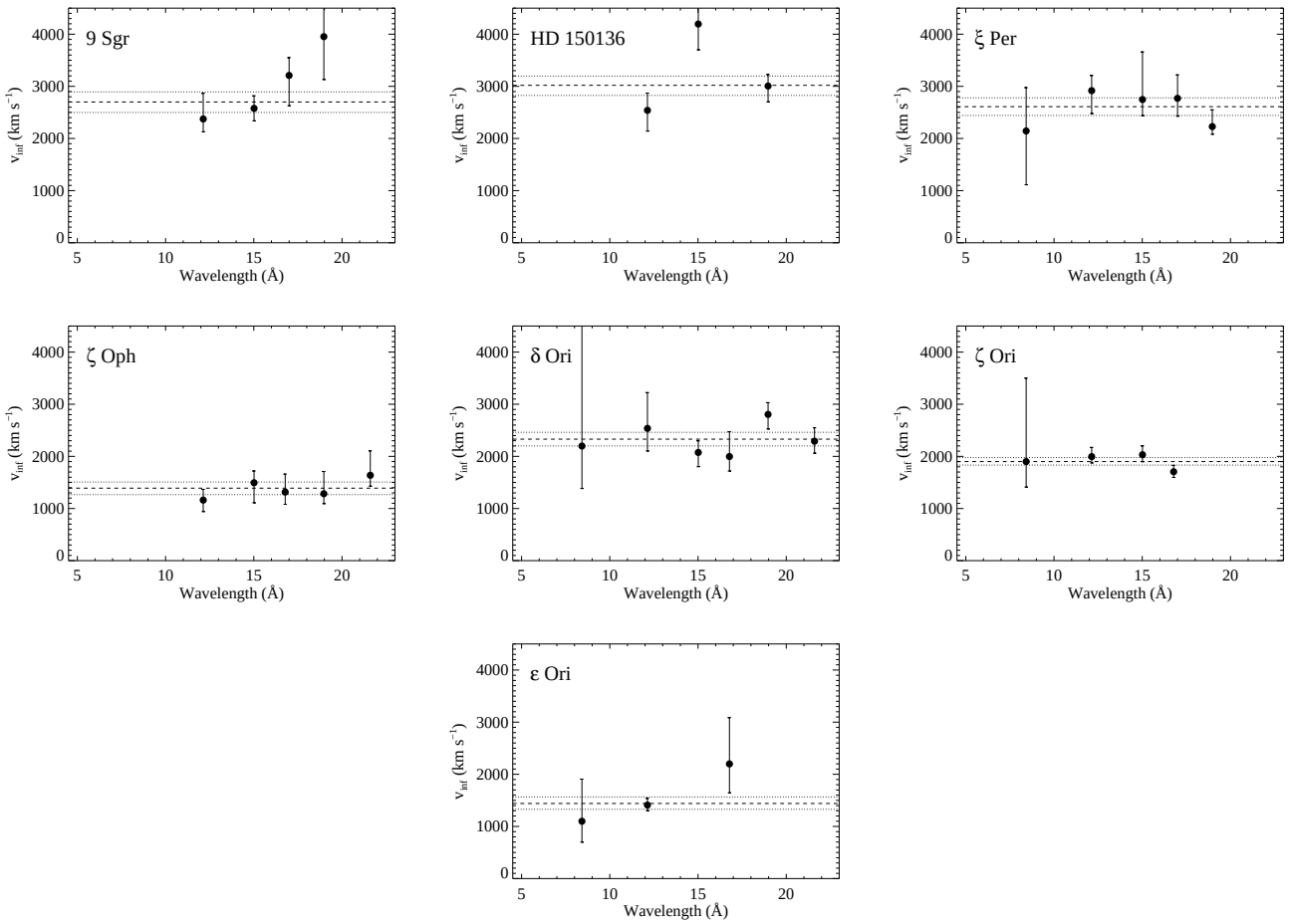

Figure 5. The fitted v_∞ values, along with the best-fit global v_∞ (dashed line) and its 68 per cent confidence limits (dotted lines).

analyzed in earlier papers using the same techniques we employ here, and are required to form a complete sample of O stars that meet our *Chandra* grating selection criteria. We will discuss the results shown in this figure further, below, but first let us consider each star in our sample, with an eye toward differentiating among the three scenarios outlined above for explaining the weaker-than-expected line profile wind absorption signatures.

5.1 Individual stars

5.1.1 HD 93250

The *Chandra* grating spectrum of this early O main sequence star is quite hard and bremsstrahlung dominated, indicating that the spectral hardness is due to high plasma temperatures rather than being a by-product of wind and ISM absorption. The early O supergiant HD 93129A simi-

Table 3. Fit Results

Star	Spectral Type	UV v_∞ (km s^{-1})	X-ray v_∞ (km s^{-1})
9 Sgr	O4 V	3100	2700^{+193}_{-201}
HD 150136	O5 III	3400	3020^{+176}_{-194}
ξ Per	O7.5 III	2450	2610^{+169}_{-168}
ζ Oph	O9 V	1550	1390^{+118}_{-124}
δ Ori	O9.5 II	2100	2330^{+132}_{-130}
ζ Ori	O9.7 Ib	1850	1900^{+77}_{-67}
ϵ Ori	B0 Ia	1600	1440^{+125}_{-112}

Co-authors: Should we also include columns for the number of lines fit and the overall χ^2 value for each star, as we do for $\dot{M}$ and R_o in the previous table?

larly has a hard X-ray spectrum, but in that star, the hardness is due almost entirely to high levels of wind and interstellar absorption (Cohen et al. 2011). HD 93250 was identified as being anomalous in X-rays in the recent Chandra Carina Complex Project (Townsley et al. 2011), with an X-ray luminosity even higher than that of HD 93129A, and a high X-ray temperature derived from low-spectral-resolution *Chandra* ACIS data (Gagné et al. 2011). Those authors suggest that the X-rays in HD 93250 are dominated by colliding wind shocks from interactions with an assumed binary companion having an orbital period greater than 30 days. Soon after the publication of that paper, Sana et al. (2011) announced an interferometric detection of a binary companion at a separation of 1.5 mas, corresponding to 3.5 AU. Thus it seems that the hard and strong X-ray spectrum and the symmetric and unshifted ($\dot{M} \approx 50\dot{M}_{\rm theory}$) X-ray emission lines can be readily explained in the context of CWS X-ray emission.

5.1.2 9 Sgr

This star is known to be a spectroscopic binary with a massive companion in an 8 or 9 year orbit (Rauw et al. 2005). The X-ray properties of 9 Sgr were described by Rauw et al. (2002) based on *XMM-Newton* observations. These authors noted blue-shifted line profiles, based on Gaussian fits, and also a somewhat higher than normal $L_{\rm X}/L_{\rm Bol}$ ratio and a moderate amount of hot ($T \approx 20$ MK) plasma based on fits to the *XMM-Newton* EPIC spectrum, although only about one per cent of the X-ray emission measure is due to this hot component. A simple CWS model computed by Rauw et al. (2002) shows that the observed X-ray emission levels cannot be explained by colliding wind shocks, and the authors conclude that the X-ray emission is dominated by embedded wind shocks. Presumably the separation of the components and/or their relative wind momenta are not optimal for producing CWS X-ray emission. It is reasonable to assume that while there may be a small amount of contamination from CWS X-rays, the line profiles we measure in the *Chandra* grating spectra are dominated by the EWS mechanism, and therefore the mass-loss rate we derive from the profile fitting is indeed a good approximation to the true mass-loss rate. We note, also, that according to the radial velocity curve shown in Rauw et al. (2005) the *Chandra* grating spectrum we analyze in this paper was taken during a phase of the orbit when the primary's radial velocity was close to zero.

5.1.3 HD 150136

A well-known spectroscopic binary, with a period of only 2.662 days (Niemela & Gamen 2005), the HD 150136 system has previously been studied in the X-ray using the same data we reanalyze here (Skinner et al. 2005). Those authors find a very high X-ray luminosity but a soft spectrum with broad X-ray emission lines. They also detect some short period X-ray variability that they tentatively attribute to an occultation effect. Although colliding wind binaries with strong X-ray emission are generally thought to produce hard X-ray emission, it has recently been shown that many massive O+O binaries have relatively soft emission and modest X-ray luminosities, especially if their orbital periods are short (Gagné et al. 2011; Gagné 2012). We also note that this star's X-ray emission stands out from the other giants and supergiants in the X-ray spectral morphology study of Walborn et al. (2009) by virtue of its high H-like/He-like silicon line ratio, indicating the presence of some hotter plasma. We conclude that although a few of the X-ray emission lines measured in this star's spectrum have non-zero τ_* values, overall the lines are too heavily contaminated by X-rays from colliding wind shocks to be used as a reliable mass-loss rate indicator.

5.1.4 Cyg OB2 8A

With phase-locked X-ray variability, a high $L_{\rm X}/L_{\rm Bol}$, and a significant amount of hot plasma with temperatures above 20 MK (De Becker et al. 2006), Cyg OB2 8A has X-ray properties characteristic of colliding wind shocks. It is a spectroscopic binary with a 21 day period in an eccentric orbit, and a semi-major axis of 0.3 AU. The small number of short-wavelength lines we are able to fit are not terribly inconsistent with the expectations of the embedded wind shock scenario, although the inferred mass-loss rate is roughly an order of magnitude lower than the theoretically expected value. However, because they are only present at short wavelengths, where the wind opacity is low, they do not provide very much leverage on the mass-loss rate, and, with their large error bars, they are also generally consistent with $\tau_* = 0$ (although the Mg XII Lyα line has $\tau_* = 0.75^{+.66}_{-.38}$). We included this star in our sample because of prior analysis of the same *Chandra* grating data in the context of a single star (Waldron et al. 2004), but given the thorough analysis by De Becker et al. (2006), we must conclude that the X-rays are dominated by colliding wind shocks, and the profile fits we present here do not provide information about embedded wind shocks or the wind mass-loss rate.

5.1.5 ξ Per

A runaway star without a close binary companion and with constant radial velocity (Sota et al. 2008), ξ Per should not have any binary colliding wind shock emission contaminating the X-ray emission lines we analyze. It does, however, show significant UV and Hα variability, at least some of which is rotationally-modulated (De Jong et al. 2001). Thus

the assumptions of spherical symmetry and a wind that is smooth on large scales is violated to some extent. Still, the X-ray line profiles should provide a relatively reliable mass-loss rate. The τ_* values we find are significantly larger than zero and are consistent with the expected wavelength trend. The mass-loss rate we derive is a factor of four or five below the theoretical value from Vink et al. (2000).

5.1.6 ι Ori

Of all the stars in the sample, ι Ori shows the least amount of line asymmetry and blue shift, with all seven lines and line complexes we analyze having τ_* values consistent with zero. Taken at face value, the derived mass-loss rate is three orders of magnitude below the theoretical value. The star is in a multiple system, with the closest component a spectroscopic binary in a highly eccentric, 29 day orbit (Bagnuolo et al. 2001). Although there are no definitive signatures of CWS X-ray emission (such as orbital modulation of the X-rays), it is very likely that the quite broad but symmetric emission lines we have measured are from colliding, rather than embedded, wind shocks.

5.1.7 ζ Oph

This star also has a nearly complete lack of wind absorption signatures in its line profiles, as shown in Fig. 3. And its lines are narrower than expected in the EWS scenario, as shown by the low R_o values in Fig. 4. Unlike the other stars in the sample with X-ray profiles that are difficult to understand in the context of embedded wind shocks, ζ Ori does not have a binary companion likely to produce colliding wind shock X-rays. It is, however, a very rapid rotator ($v \sin i = 351$ km s^{-1} (Conti & Ebbets 1977)), goes through Hα emission episodes that qualify it as an Oe star (Barker & Brown 1974), and has an equatorially concentrated wind (Massa 1995). The wind's deviation from spherical symmetry could explain the relatively symmetric and narrow X-ray emission lines, most likely through alterations to the line-of-sight velocity distribution of the emitting plasma in the wind.

5.1.8 δ Ori

With a quite small amount of wind attenuation evident in its line profiles and narrower than expected lines, the results from δ Ori are also suspect, although there are some emission lines with non-zero τ_* values in its *Chandra* spectrum. This star is a member of a multiple system that includes an eclipsing, spectroscopic binary companion with an orbital period of 5.7 days. The companion is an early B star, and an earlier analysis of these same *Chandra* data indicated that colliding wind shocks were not likely to be strong enough to account for the X-ray luminosity of $L_X \approx 10^{32}$ ergs s^{-1} (Miller et al. 2002). However, given the uncertainty in the companion's wind properties as well as general uncertainties in the CWS model's X-ray emission predictions, it seems quite likely that a significant fraction of the observed X-ray line emission arises in the wind-wind interaction zone between the late O star and its early B companion.

5.1.9 ζ Ori

Significant wind absorption signatures are seen in the X-ray profiles of ζ Ori (as demonstrated in Cohen et al. (2006)), which has the highest signal-to-noise *Chandra* spectrum of any of the stars in our sample. The expected wavelength trend is seen in the τ_* results, especially after the O Lyα and He$_\alpha$ lines are excluded due to resonance scattering. The fitted R_o values are consistent with $R_o = 1.5\ R_*$, expected in the embedded wind shock scenario. While it is possible that there could be some contamination from CWS X-ray emission, the binary companion of ζ Ori is two magnitudes fainter than the primary and is at a separation of about 10 AU, making strong CWS emission an unlikely scenario (Hummel et al. 2000; Rivinius et al. 2011).

5.1.10 ϵ Ori

The only B star in our sample, ϵ Ori is a B0Ia MK standard, and given its evolved state and high luminosity, its wind is as strong as many of the O stars in our sample. Nearly all of the X-ray emission lines show wind signatures with τ_* values that deviate significantly from zero. It is also the only star in our sample for which eliminating the lines most likely subject to resonance scattering has a very significant effect on our derived mass-loss rate, increasing it from 2.1×10^{-7} M$_\odot$ yr^{-1} to 6.4×10^{-7} M$_\odot$ yr^{-1}. Eliminating those lines also significantly improves the mass-loss rate fit to the τ_* values, further indicating that they are indeed subject to resonance scattering. And the low wind terminal velocity of ϵ Ori makes resonance scattering Sobolev optical depths larger, all things being equal, so the importance of the effect here, but not apparently in most of the other stars, is reasonable. Thus, we report the higher mass-loss rate in Table 2 and show the fit from which that value is derived in Fig 3. There is no reason to believe that CWS X-ray emission affects the star's *Chandra* spectrum. Its only known companion is at 3′ (Halbedel 1985) (which would be easily resolved by *Chandra*) but is not seen in the *Chandra* data, while interferometric observations show no binary companion down to small separations (Richichi & Percheron 2002).

5.2 Discussion

Taking the X-ray profile information we have analyzed here, along with knowledge of the multiplicity and other properties of the sample stars, it seems that about half of the stars in the sample have some significant contamination of their X-ray profiles from colliding wind shock X-ray emission due to the interaction of their winds with those from binary companions. CWS X-ray emission is generally considered to be harder and stronger than that from embedded wind shocks, but that seems to be the case primarily in systems where both components have very strong winds with relatively closely matched wind momenta. Furthermore, systems with short periods often lack hard X-rays emission and the expected X-ray over-luminosity (Gagné 2012), and thus might not be immediately obvious as CWS-dominated systems based on a snapshot of their X-ray spectral energy distributions. Furthermore, while idealized CWS models predict distinctive X-ray emission line profile shapes (Henley et al. 2003), such shapes are not observed in real systems

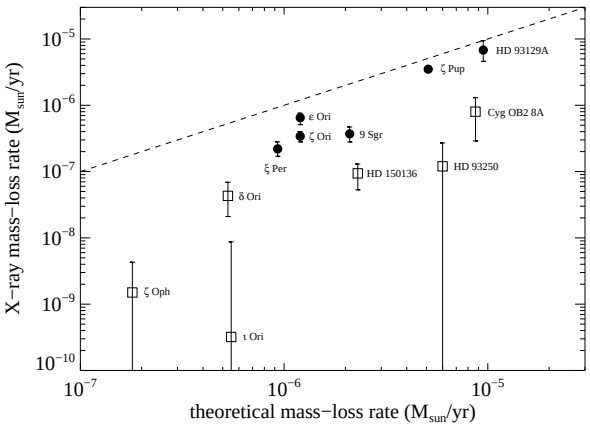

Figure 6. The X-ray derived mass-loss rates for each star in our sample (and also ζ Pup and HD 93129A) compared to the theoretically expected mass-loss rate from Vink et al. (2000). Stars dominated by EWS are shown as filled circles, while those where our model breaks down, in most cases due to CWS X-rays, are shown as open squares.

(e.g. Henley et al. (2005)), perhaps because of shock instabilities and the associated mixing and large random velocity components of the X-ray emitting plasma (Pittard & Parkin 2010). Therefore, when a mixture of CWS and EWS X-rays are present, the observed, hybrid line profiles should be relatively symmetric and moderately broad, mimicking pure EWS profiles with little or no absorption.

The three earliest O stars in our sample where we suspect CWS X-ray contamination do in fact have X-ray properties that are quite different than normal O stars dominated by EWS X-ray emission. HD 93250, HD 150136, and Cyg OB2 8A are overluminous in the X-ray and/or have unusually hard X-ray emission. All three have O star binary companions with separations likely to lead to enhanced CWS X-ray emission. The later O stars where we suspect binary CWS contamination, ι Ori and δ Ori, have overall X-ray emission levels and temperatures that are not far out of line with those expected from EWS sources. But they do have close, massive binary companions and X-ray line properties that are inconsistent with a purely EWS origin. It is possible that they are only partially contaminated by CWS emission (perhaps this is the case, too, for HD 150136, where some of the X-ray emission lines also show non-zero τ_* values).

While the five stars mentioned above all seem to fall into case (2) enumerated in the opening of this section – contamination of the observed X-rays by a process other than the EWS mechanism – the other object with results difficult to interpret in the EWS framework likely falls into case (1), a breakdown of the assumptions in our simple X-ray line profile model. That object is ζ Oph, for which there is strong evidence for a non-spherical wind. Because the line profile model we employ assumes spherical symmetry and the resulting geometry and kinematics governs the manifestation of wind attenuation in the line profiles, we cannot interpret the derived τ_* values in terms of wind attenuation for this star. *(Co-authors: Or is this maybe just a very weak-wind star?)*

The remaining stars in the sample: 9 Sgr, ξ Per, ζ Ori, and ϵ Ori have X-ray profiles that are consistent with the expectations of the EWS scenario, with significant wind attenuation evident from the fitted τ_* values, which also show the expected wavelength trend of longer-wavelength lines having larger optical depths due to the greater wind opacity at those wavelengths. These stars have fitted R_o values of $R_o \approx 1.5\ R_*$, or a little above, confirming the predictions of LDI simulations of embedded wind shocks (Feldmeier et al. 1997; Runacres & Owocki 2002). We note that if $\beta < 1$, then the derived R_o values will be modestly lower (Cohen et al. 2010a). This is the case for 9 Sgr, which when fit with $\beta = 0.7$ gives $R_o = 1.4$ (Cohen et al. 2010b).

We note also that there is some evidence for longer wavelength lines (which are formed in cooler plasma than are shorter wavelength lines) having larger R_o in ζ Oph, δ Ori, ζ Ori, and ϵ Ori. For the latter two, where the X-ray seem to arise in standard embedded wind shocks, this might be expected through some combination of the fact that any given shock-heated parcel will cool as it moves downstream and the tendency seen in simulations of the self-excited LDI for the shock velocity dispersion to decrease with radius (Runacres & Owocki 2002). For the other two stars, the larger derived R_o values are harder to interpret, and essentially just parametrize slightly larger line-widths. *Co-authors: I will fit a linear and maybe quadratic function to the Ro vs. lambda data.*

The fitted values of v_∞ also constrain the kinematics of the shock-heated wind plasma, confirming the general picture in which the X-ray emitting wind's terminal velocity is consistent with the terminal velocities of their bulk, UV absorbing winds (with 9 Sgr being discrepant at 2σ). The 1-D LDI simulations generally show this behavior (Runacres & Owocki 2002). *Co-authors/Stan: I think you called this a "red-herring" recently, given that we think the clump-clump collisions produce the bulk of the X-rays. (Since the clumps "are the wind" maybe we can just appeal to a statistical averaging over the clump velocity dispersion-distribution to justify the common kinematics of the hot and cold wind components, at least for radiative shocks.)*

Of the four stars in this study with reliable X-ray mass-loss rates and the two from previous studies, we find mass-loss rates that range from being slightly less than theoretical predictions (ϵ Ori, ζ Pup, HD 93129A) to about six times less (9 Sgr). The discrepancy seems to be worse for stars with lower theoretical mass-loss rates. *Co-authors: Is there more we can say to put the low mass-loss rates and the discrepancies with Vink in perspective? How plausible is it that the Vink rates are consistently off by ~ 5? What's the connection to the "weak-wind problem"?*

Below are several topics that we could consider addressing and things we could add to the paper.

The issue of adiabatic vs. radiative shocks.

Should we show more data? We could put all the line fits for the four "good" stars in an appendix. We could also show poorly fitting lines and lines of interest (e.g. the Cyg OB2 8A line with a non-zero τ_*).

Should we make any direct comparisons to Waldron and Cassinelli (2007)? We could point out the lack of evidence for extremely small R_o among the f/i ratios we analyze.

What about comparisons with other diagnostics (and thus insights about clumping and clumping factors)? And comments on the Hα *profile properties themselves (maybe emphasizing how none of the sample stars really have* Hα *in emission nor is the emission component constant)? Should we analyze any of the* Hα *profiles? Jon, Janos, Alex?*

How about comments/conclusions on the utility of X-ray mass-loss rates diagnostics (there aren't many more stars where this technique can be applied with current instrumentation, but we can provide motivation for future high-resolution X-ray missions, and maybe also make connections to broadband X-ray mass-loss rate diagnostics (i.e. windtabs))?

Seems like there's interesting results related to the rejected, or suspect, stars (e.g. broad, symmetric lines for some CWS systems; hybrid CWS/EWS spectra) – *should we discuss that more?* We've already noted twice that δ Ori and HD 150136 may be hybrid cases.

I'm planning on refitting the $\dot{\rm M}$ for ζ Pup, using the same wind opacity model we use for all the stars in this paper. It will go down a bit from the published $\dot{\rm M} = 3.5 \times 10^{-6}$.

ACKNOWLEDGMENTS

Support for this work was provided by the National Aeronautics and Space Administration through *Chandra* award numbers AR7-8002X and AR0-11002B to Swarthmore College. EEW was supported by a Lotte Lazarsfeld Bailyn Summer Research Fellowship from the Provost's Office at Swarthmore College. JOS and SPO acknowledge support from NASA award ATP NNX11AC40G to the University of Delaware.

REFERENCES

Asplund M., Grevesse N., Sauval A. J., Scott P., 2009, ARAA, 47, 481
Bagnuolo W. G., Riddle R. L., Gies D. R., Barry D. J., 2001, ApJ, 554, 362
Barker P. K., Brown T., 1974, ApJ, 192, L11
Bouret J. C., Lanz T., Hillier D. J., 2005, A&A, 438, 301
Canizares C. R., et al., 2005, PASP, 117, 1144
Cash W., 1979, ApJ, 228, 939
Cassinelli J. P., Miller N. A., Waldron W. L., MacFarlane J. J., Cohen D. H., 2001, ApJ, 554, L55
Cohen D. H., Gagné M., Leutenegger M. A., MacArthur J. P., Wollman E. E., Sundqvist J. O., Fullerton A. W., Owocki S. P., 2011, MNRAS, 415, 3354
Cohen D. H., Kuhn M. A., Gagné M., Jensen E. L. N., Miller N. A., 2008, MNRAS, 386, 1855
Cohen D. H., Leutenegger M. A., Wollman E. E., Zsargó J., Hillier D. J., Townsend R. H. D., Owocki S. P., 2010, MNRAS, 405, 2391
Cohen D. H., Leutenegger M. A., Grizzard K. T., Reed C. L., Kramer R. H., Owocki S. P., 2006, MNRAS, 368, 1905
Cohen D. H., Wollman E. E., Leutenegger M. A., 2010, *IAU Symposium 272*, eds. C. Neiner, G. Wade, G. Meynet, G. Peters, 348
Conti P. S., Ebbets D., 1977, ApJ, 213, 438
De Becker M., Rauw G., Sana H., Pollock A. M. T., Pittard J. M., Blomme R., Stevens I. R., van Loo S., 2006, MNRAS, 371, 1280
de Jong J. A., et al., 2001, A&A, 368, 601
Feldmeier A., Puls J., Pauldrach A. W. A., 1997, A&A, 322, 878
Fullerton A. W., Massa D. L., Prinja R. K., 2006, ApJ, 637, 1025
Gagné M., et al., 2011, ApJS, 194, 5
Gagné M., 2012, (arXiv:)
Halbedel E. M., 1985, PASP, 97, 434
Hamann W.–R., Feldmeier A., Oskinova L. M., 2008, Clumping in Hot Star Winds. Universitatsverlag, Potsdam
Henley D. B., Stevens I. R., Pittard J. M., MNRAS, 346, 773
Henley D. B., Stevens I. R., Pittard J. M., MNRAS, 356, 1308
Hoogerwerf R., de Bruijne J. H. J., de Zeeuw P. T., 2001, A&A, 365, 49
Hummel C. A., White N. M., Elias N. M., Hajian A. R., Nordgren T. E., 2000, ApJ, 540, L91
Kahn S. M., Leutenegger M. A., Cottam J., Rauw G., Vreux J.–M., den Boggende A. J. F., Mewe R., Güdel M., 2001, A&A, 365, L312
Lanz T., Hubeny I., 2003, ApJS, 146, 417
Leutenegger M. A., Cohen D. H., Sundqvist J. O., Owocki S. P., 2012, MNRAS, submitted
Leutenegger M. A., Owocki S. P., Kahn S. M., Paerels F. B. S., 2007, ApJ, 659, 642
Leutenegger M. A., Paerels F. B. S., Kahn S. M., Cohen D. H., 2006, ApJ, 650, 1096
MacFarlane, J. J., Cohen D. H., Wang P., 1994, ApJ, 437, 351
Mauche C. W., Liedahl D. A., Fournier M. B., 2001, ApJ, 560, 992
Massa D., 1995, ApJ, 438, 376
Miller N. A., Cassinelli J. P., Waldron W. L., MacFarlane J. J., Cohen D. H., 2002, ApJ, 577, 951
Niemela V. S., Gamen R. C., 2005, MNRAS, 356, 974
Oskinova L., Feldmeier A., Hamann W.–R., 2006, MNRAS, 372, 313
Owocki S. P., Cohen D. H., 2001, ApJ, 559, 1108
Owocki S. P., Cohen D. H., 2006, ApJ, 648, 565
Pittard J. M., Parkin E. R., 2010, MNRAS, 403, 1657
Press W. H., Flannery B. P., Teukolsky S. A., Vetterling W. T., 2007, Numerical Recipes, 3^{rd} edition. Cambridge University Press, Cambridge
Puls J., Markova N., Scuderi S., Stanghellini C., Taranova O. G., Burnley A. W., Howarth I. D., 2006, A&A, 454, 625
Rauw G., Sana H., Gosset E., De Becker M., Arias J., Morrell N., Eenens P., Stickland D., 2005, in "Massive Stars and High-Energy Emission in OB Associations," eds. G. Rauw, Y. Nazé, R. Blomme, & E. Gosset, Liege: JENAM, 85
Rauw G., Blomme R., Waldron W. L., Corcoran M. F., Pittard J. M., Pollock A. M. T., Runacres M. C., Sana H., Stevens I. R., Van Loo S., 2002, A&A, 394, 993
Repolust T., Puls J., Herrero A., 2004, A&A, 415, 349
Richichi A., Percheron I., 2002, A&A, 386, 492
Rivinius T., Hummel C. A., Stahl O., 2011, IAUS, 272, 539
Runacres M. C., Owocki S.P., 2002, A&A, 381, 1015
Sana H.., Le Bouquin J.-B., De Becker M., Berger J.-P., de Koter A., Mérand A., 2011, ApJ, 740, L43
Skinner S. L., Zhekov S. A., Palla F., Barbosa C. L. D. R., 2005, MNRAS, 361, 191
Skinner S. L., Sokal K. R., Cohen D. H., Gagné M., Owocki S. P., Townsend R. D., 2008, ApJ, 683, 796
Sota A., Maíz Apellániz J., Walborn N. R., Shida R. Y., 2008, Rev. Mex., 33, 56
Stevens I. R., Blondin J. M., Pollock A. M. T., 1992, ApJ, 386, 265
Sundqvist J. O., Owocki S. P., Cohen D. H., Leutenegger M. A., Townsend R. H. D., 2012, MNRAS, 420, 1553
Townsley L., et al., 2011, ApJS, (arXiv:1102.4779)
Vink J., de Koter A., Lamers H. J. G. L. M., 2000, A&A, 362, 295
Walborn N. R., Nichols J. S., Waldron W. L., 2009, ApJ, 703, 633
Waldron W. L., Cassinelli J. P., Miller N. A., MacFarlane J. J., Reiter J. C., 2004, ApJ, 616, 542
Westbrook O. W., et al., 2008, ApJS, 176, 218